Compression of hyperspectral remote sensing images by tensor approach

Lefei Zhang [a], Liangpei Zhang [b], Dacheng Tao [c], Xin Huang [b], Bo Du [a,*]

[a] Computer School, Wuhan University, Wuhan 430072, China
[b] State Key Laboratory of Information Engineering in Surveying, Mapping, and Remote Sensing, Wuhan University, Wuhan 430079, China
[c] Centre for Quantum Computation and Intelligent Systems, Faculty of Engineering and Information Technology, University of Technology, Sydney, NSW 2007, Australia

ARTICLE INFO

ABSTRACT

Whereas the transform coding algorithms have been proved to be efficient and practical for grey-level and color images compression, they could not directly deal with the hyperspectral images (HSI) by simultaneously considering both the spatial and spectral domains of the data cube. The aim of this paper is to present an HSI compression and reconstruction method based on the multi-dimensional or tensor data processing approach. By representing the observed hyperspectral image cube to a 3-order-tensor, we introduce a tensor decomposition technology to approximately decompose the original tensor data into a core tensor multiplied by a factor matrix along each mode. Thus, the HSI is compressed to the core tensor and could be reconstructed by the multi-linear projection via the factor matrices. Experimental results on particular applications of hyperspectral remote sensing images such as unmixing and detection suggest that the reconstructed data by the proposed approach significantly preserves the HSI's data quality in several aspects.

© 2014 Elsevier B.V. All rights reserved.

1. Introduction

Remotely sensed images, which are acquired by the airborne or spaceborne sensors, have been extensively used in earth observation applications. Hyperspectral imaging sensors can collect an image in which each pixel has the contiguous bands of spectra, and these large number of spectral channels provide the opportunity for the detailed analysis of the land-cover materials [1], e.g., endmember extraction [2,3], spectral unmixing [4,5], target detection [6–8], image classification [9–11], and so on . However, as the hyperspectral image (HSI) is intrinsically a data cube which has two spatial dimensions (width and height) and a spectral dimension, numerous researches have indicated that the redundancy from both inter-pixel and inter-band correlation is very high and thus the data cube could be compressed by some algorithms without a significant loss of the useful information for subsequent HSI analysis [12,13].

Generally, image compression technologies can significantly reduce the HSI volumes to a more manageable size for storage and communication. In the literature, most of the existing HSI compression

algorithms are transform coding based approaches, e.g., Set Partitioning in Hierarchical Trees (SPIHT) and Set Partitioned Embedded bloCK (SPECK) algorithms [14], the progressive 3-D coding algorithm [15], the 3-D reversible integer lapped transform [16], and the discrete wavelet transform coupled with tucker decomposition [17], etc. Also based on the wavelet transform, Du et al. proposed a series of works on using JPEG 2000 ISO standard for HSI compression, the most important of which are JPEG2000 and Principal Component Analysis (PCA) based HSI compression methods [12,18,19]. As suggested in the aforementioned papers, the transform coding has been proved efficient and practical for HSI compression. However, most of the transform coding related algorithms were originally designed to process 2-D grey-level images, and then extended to 3-D data cube without the consideration of special characteristics of HSI, which might be problematic when the subsequent image analysis is conducted on the reconstructed HSI cube [12,20].

In this paper, we propose a method for compression of the HSIs in a novel point of view, which is based on the multi-dimensional or tensor data processing approach [21–25]. As indicated in some previous works within the hyperspectral imaging area, an HSI data can be intrinsically treated as a 3-order-tensor, by this way the data structure of both the spatial and spectral domains is well preserved [26,27]. For the task of HSI compression, by representing the observed HSI data cube to a 3-order-tensor with two spatial modes and an

* Corresponding author.
  E-mail address: gunspace@163.com (B. Du).

additional spectral mode, we introduce a tensor decomposition technology to decompose the original tensor into a core tensor with same order while much lower dimensionality multiplied by a matrix along each mode, under the umbrella of multi-linear algebra, i.e., the algebra of tensors. Thus, the HSI is compressed to the core tensor, and the reconstructed HSI is actually a low-rank tensor which could be acquired by the multi-linear backward projection via the factor matrices. HSI compression and reconstruction experiments on two public data sets show that the proposed method not only obtains the highest PSNR value, but also significantly preserves the HSI data quality which is benefit for several subsequent image analysis including the endmember extraction, spectral unmixing, and target detection.

The remainder of this paper is organized as follows. In the following section, we give a brief description of related tensor algebra, and then presents the proposed HSI compression algorithm in detail. After that, the experiments are reported in Section 3, followed by the conclusion.

2. The proposed HSI compression algorithm

The notations used in this paper are followed by convention in the multi-linear algebra, e.g., vectors are denoted by lowercase boldface and italic letters, such as $\boldsymbol{x}$, matrices by uppercase boldface and italic, such as $\boldsymbol{U}$, and tensors by calligraphic letters, such as $\mathcal{X}$. For a K-order-tensor $\mathcal{X} \in \mathrm{R}^{L_1 \times L_2 \times \cdots \times L_K}$, where L_i shows the size of this tensor in each mode, and the elements of $\mathcal{X}$ are denoted with indices in lowercase letters, i.e., $\mathcal{X}_{l_1, l_2, \ldots, l_K}$, in which each l_i addresses the i-mode of $\mathcal{X}$, and $1 \le l_i \le L_i$, $i \in (1, 2, \ldots, K)$. Unfolding $\mathcal{X}$ along the i-mode is defined by keeping the index l_i fixed and varying the other indices, the result of which is denoted as $\mathcal{X}_{(i)} \in \mathrm{R}^{L_i \times \prod_{j \ne i} L_j}$. The i-mode product of a tensor $\mathcal{X}$ by a matrix $\boldsymbol{U} \in \mathrm{R}^{J_i \times L_i}$, is a tensor with entries $(\mathcal{X} \times_i \boldsymbol{U})_{l_1, \ldots, l_{i-1}, j_i, l_{i+1}, \ldots, l_K} = \sum_{l_i} \mathcal{X}_{l_1, \ldots, l_K} \boldsymbol{U}_{j_i, l_i}$. The Frobenius norm of a tensor $\mathcal{X}$ is given by $\|\mathcal{X}\| = \sqrt{\sum_{l_1} \cdots \sum_{l_K} \mathcal{X}^2_{l_1, l_2, \ldots, l_K}}$, and the Euclidean distance between two tensors $\mathcal{X}$ and $\mathcal{Y}$ could be measured by $\|\mathcal{X} - \mathcal{Y}\|$. For more detailed information, refer to [21,28–30].

As discussed above, in order to preserve the most representative information of the HSI data, we denote the data cube as a 3-order-tensor $\mathcal{X} \in \mathrm{R}^{L_1 \times L_2 \times L_3}$, in which L_1, L_2, and L_3 give the height, width and spectral channels of HSI, respectively. Then, the compressed tensor $\mathcal{C}$ (also known as the core tensor of $\mathcal{X}$) can be acquired by the following multi-linear projection:

$$\mathcal{C} = \mathcal{X} \times_1 \boldsymbol{U}_1 \times_2 \boldsymbol{U}_2 \times_3 \boldsymbol{U}_3 \tag{1}$$

in which $\boldsymbol{U}_1 \in \mathrm{R}^{J_1 \times L_1}$, $\boldsymbol{U}_2 \in \mathrm{R}^{J_2 \times L_2}$, and $\boldsymbol{U}_3 \in \mathrm{R}^{J_3 \times L_3}$ are series of projection matrices and $J_i \le L_i$, $i \in (1, 2, 3)$. By this way, $\mathcal{X}$ is compressed to $\mathcal{C} \in \mathrm{R}^{J_1 \times J_2 \times J_3}$ with the rate of $\prod_{i=1}^3 J_i / \prod_{i=1}^3 L_i$, and the reconstructed tensor could be acquired by the following multi-linear projection:

$$\hat{\mathcal{X}} = \mathcal{C} \times_1 \boldsymbol{U}_1^\mathrm{T} \times_2 \boldsymbol{U}_2^\mathrm{T} \times_3 \boldsymbol{U}_3^\mathrm{T}. \tag{2}$$

The reconstructed tensor $\hat{\mathcal{X}}$ given in (2) is in fact a low-rank tensor, thus the reconstruction error $\mathcal{E}$ could be computed by

$$\mathcal{E} = \mathcal{X} - \hat{\mathcal{X}}. \tag{3}$$

As an effective HSI compression algorithm, we expect that the reconstructed tensor $\hat{\mathcal{X}}$ should be close to the original tensor data $\mathcal{X}$ as much as possible. According to this aspect, the required projection matrices $\boldsymbol{U}_i$, $i \in (1, 2, 3)$ should be optimized by minimizing the Euclidean distance between $\mathcal{X}$ and $\hat{\mathcal{X}}$, which also could be written as the Frobenius norm of $\mathcal{E}$:

$$\arg \min_{\boldsymbol{U}_1, \boldsymbol{U}_2, \boldsymbol{U}_3} \|\mathcal{X} - \hat{\mathcal{X}}\|^2 = \arg \min_{\boldsymbol{U}_1, \boldsymbol{U}_2, \boldsymbol{U}_3} \|\mathcal{E}\|^2. \tag{4}$$

By combining (1), (2) into (4), we have the following optimization of the proposed HSI compression algorithm:

$$\arg \min_{\boldsymbol{U}_1, \boldsymbol{U}_2, \boldsymbol{U}_3} \|\mathcal{X} - \mathcal{X} \times_1 \boldsymbol{U}_1^\mathrm{T} \boldsymbol{U}_1 \times_2 \boldsymbol{U}_2^\mathrm{T} \boldsymbol{U}_2 \times_3 \boldsymbol{U}_3^\mathrm{T} \boldsymbol{U}_3\|^2. \tag{5}$$

Eq. (5) presents the same form with a tensor decomposition technology, i.e., the Tucker decomposition [30,31], which is a form of higher-order PCA and aims to decompose a tensor into a core tensor transformed by a factor matrix along each mode. Thus we abbreviate the proposed method as "TenD" in the rest of this paper. The objective function of (5) could be locally optimized by alternating optimization. The basic idea of this solution comes from the fact that any one of the projection matrix could be simply acquired by an eigenvalue decomposition problem when the remaining two matrices are fixed. So, after initializing $\boldsymbol{U}_i$, $i \in (1, 2, 3)$, the optimal projection matrices along all modes can be acquired iteratively.

Specifically, the projection matrices could be initialized as either identity matrices or arbitrary columnly-orthogonal matrices. In this paper, we suggest to use the higher-order SVD (HOSVD) [30] to find a good starting point for an alternating optimization. Then, the higher-order orthogonal iteration (HOOI) [31] is used to optimize $\boldsymbol{U}_i$, $i \in (1, 2, 3)$ in an iterative way. The detailed procedure for solve Eq. (5) is given below.

Algorithm 1. Procedure to solve TenD.

> **Input**: Input HSI data $\mathcal{X} \in \mathrm{R}^{L_1 \times L_2 \times L_3}$ and compressed dimensionality in each mode J_1, J_2 and J_3;
> **Initialize** $\boldsymbol{U}_i$, $i \in (1, 2, 3)$ using HOSVD;
> **repeat**
> - $\mathcal{C} = \mathcal{X} \times_2 \boldsymbol{U}_2 \times_3 \boldsymbol{U}_3$, let $\boldsymbol{U}_1$ be the J_1 leading left singular vectors of $\mathcal{C}_{(1)}$;
> - $\mathcal{C} = \mathcal{X} \times_1 \boldsymbol{U}_1 \times_3 \boldsymbol{U}_3$, let $\boldsymbol{U}_2$ be the J_2 leading left singular vectors of $\mathcal{C}_{(2)}$;
> - $\mathcal{C} = \mathcal{X} \times_1 \boldsymbol{U}_1 \times_2 \boldsymbol{U}_2$, let $\boldsymbol{U}_3$ be the J_3 leading left singular vectors of $\mathcal{C}_{(3)}$;
> **until** Convergence
> **Output**: Projection matrices $\boldsymbol{U}_1$, $\boldsymbol{U}_2$ and $\boldsymbol{U}_3$ for HSI compression.

It is worth noting that some representative HSI spectral dimension reduction (DR) algorithms, e.g., PCA and maximum noise fraction (MNF) [32,33], could also perform HSI compression and reconstruction but only in the spectral domain. This branch of approaches considers the HSI data as a set of spectral feature vectors $\boldsymbol{x}_i \in \mathrm{R}^{L_3} | i = [1, \ldots, L_1 L_2]$ in which L_3 gives the spectral channels and $L_1 L_2$ is the number of pixels in HSI. Then, the DR algorithm outputs the linear projection matrix $\boldsymbol{U} \in \mathrm{R}^{d \times L_3}$ ($d \le L_3$) by some certain criterions, e.g., PCA finds the principal components in accordance with the maximum variance of the data and MNF transforms the principal components which are ranked by SNR. Similar to tensor compression (1), the low-dimensional feature representation $\boldsymbol{y}_i \in \mathrm{R}^d$ (here the compression rate is d/L_3) is obtained by

$$\boldsymbol{y}_i = \boldsymbol{U} \times \boldsymbol{x}_i, \quad i = [1, \ldots, L_1 L_2] \tag{6}$$

and the reconstructed feature vector could be recovered by the backward projection:

$$\hat{\boldsymbol{x}}_i = \boldsymbol{U}^\mathrm{T} \times \boldsymbol{y}_i, \quad i = [1, \ldots, L_1 L_2]. \tag{7}$$

Obviously, Eqs. (6) and (7) consider the feature redundancy in the spectral domain while ignore the cross-domain redundancy of the input HSI data. Correspondingly, the proposed TenD algorithm deals with the HSI data by simultaneously considering both the spatial and spectral domains of the data cube, which can make
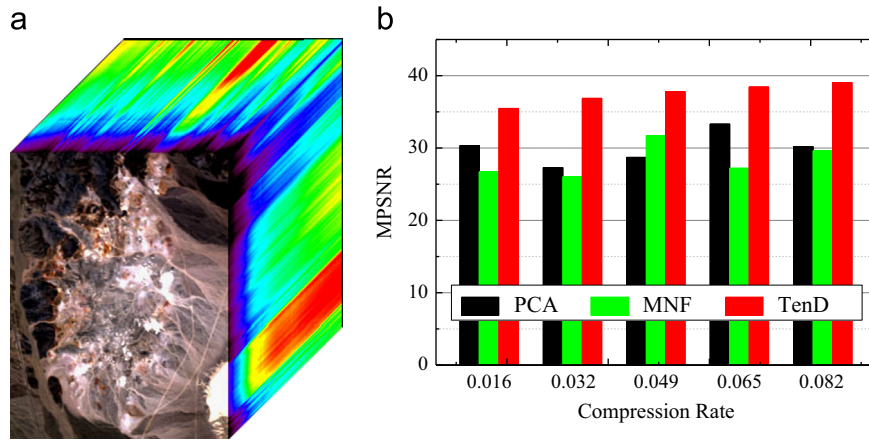
Fig. 1. (a) AVIRIS data cube (bands 28, 19, and 10 for red, green, and blue, respectively); (b) MPSNR values with respect to various compression rates in AVIRIS data cube. (For interpretation of the references to color in this figure caption, the reader is referred to the web version of this article.)
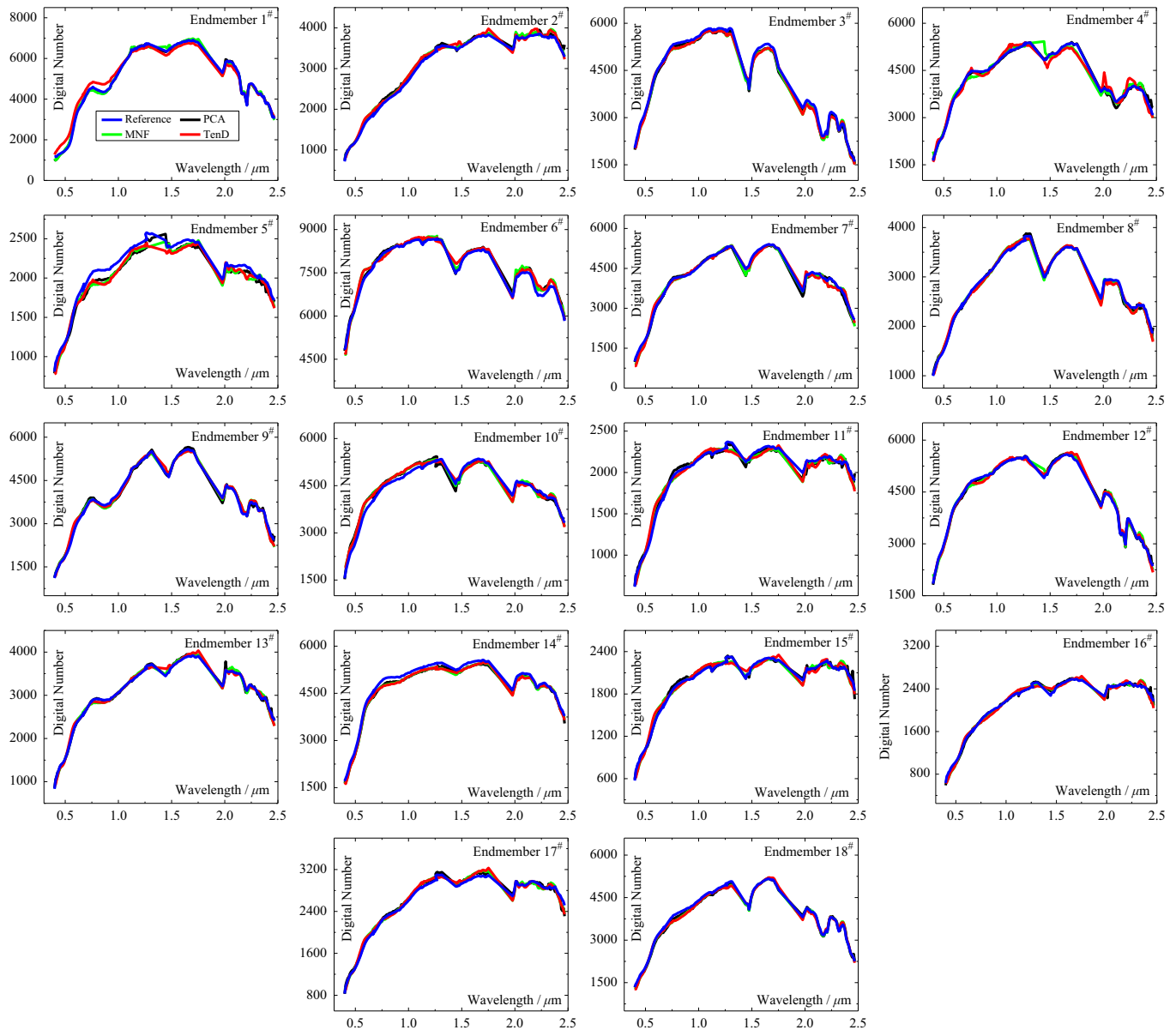

Fig. 2. About 18 endmembers extracted from the original AVIRIS data cube and the reconstructed data cube by three algorithms.

sure that the significant data quality in HSI could be preserved as complete as possible as shown in the following experimental reports.

3. Experiments and analysis

In this section, two public benchmark HSIs are used to demonstrate the superiority of the proposed TenD algorithm in several aspects. Since the particular advantage of the TenD algorithm lies in that it considers the hyperspectral image as a whole 3-order-tensor data rather than the series of vectors, therefore, we compare it to PCA and MNF which consider the HSI data as a set of spectral feature vectors and then perform the HSI compression and reconstruction only in the spectral domain. The first dataset is the Airborne Visible Infrared Imaging Spectrometer (AVIRIS) Cuprite hyperspectral image, which had been extensively investigated by researchers and actually serves as the standard data for HSI endmember extraction and spectral unmixing. The second one is a HyMap image provided by the Rochester Institute of Technology (RIT) self-test project [34]. This dataset was particularly designed for target detection and equipped with the exact locations and Spectral Library (SPL) files of all the desired targets. Therefore, it is also one of the standard datasets for hyperspectral target detection algorithms.

3.1. Performance on AVIRIS data set

The AVIRIS data cube is shown in Fig. 1(a), this data cube includes 190 lines, 250 rows, and 182 spectral channels. In order to comprehensively evaluate the HSI compression performance, we show the reconstructed HSI quality respect to various compression rates. In detail, we select $d = [3, 6, 9, 12, 15]$ in PCA and MNF to plot Fig. 1(b) and the compression parameters J_1, J_2 and J_3 in TenD are set in line with the certain compression rate. The Mean Peak Signal to Noise Ratio (MPSNR) value is introduced to measure the quality of the reconstructed HSI by comparing it with the original HSI data. Fig. 1(b) shows the MPSNR values regarding the various compression rates by PCA, MNF and proposed TenD algorithms. It is obvious that TenD algorithm achieves the best HSI reconstruct quality in all of the compression rates.

We hereby use the AVIRIS data set to show the effect of the HSI compression algorithms on endmember extraction and spectral unmixing. In this experiment, the compression rate of all algorithms is fixed at 0.049. Firstly, the endmembers extracted from the original HSI data as well as their locations are recorded as the reference. In this step, the number of endmembers is estimated as 18 by the HySime [35] algorithm while the endmembers are extracted by the Vertex Component Analysis [36] algorithm. Then, we compare the endmember pixels at the recorded locations of the reconstructed HSIs with the reference, the detailed spectral curves of 18 endmember pixels are plotted in Fig. 2. It is obvious that the curves provided by TenD algorithm have the similar shape

to the reference curves in all of the sub-figures. The quantitative comparison of the endmember extraction results are measured by the spectral angle mapper (SAM), as given in Table 1, the proposed TenD algorithm outperforms PCA and MNF in 14 endmembers of all the 18 ones in the reference.

Finally, we use the endmembers in reference to perform spectral unmixing of the original HSI cube and the reconstructed cubes, by the Un-Constrained Least Squares (UCLS) abundance estimation method. The Root Mean Squared Error (RMSE) is adopted as the metric to compare the performance. As indicated in Table 2, the proposed TenD algorithm performs better than PCA and MNF.

3.2. Performance on HyMap data set

Fig. 3 shows the HyMap data cube of the RIT project, with a size of $280 \times 800 \times 126$. In the HyMap experiment, we also firstly show MPSNR values of the reconstructive HSIs with respect to various compression rates (see Fig. 4(a)). Since we experimentally observe that this data cube can be compressed to some lower rates than the AVIRIS data cube, we select $d = [3, 6, 9, 12, 15]$ in PCA and MNF to plot Fig. 4(a) and the compression parameters J_1, J_2 and J_3 in TenD are set in line with the certain compression rate. Similar to the technical indices reported in the previous subsection, we observe that the proposed algorithm outperforms the comparison approaches at all the compression rates.

The target detection is performed on both the original and reconstructed HSIs by a famous hyperspectral detector, i.e., the adaptive cosine estimator (ACE) [37]. The compressed rate is fixed to even a little lower than the AVIRIS experiment (0.015). According to the RIT project [34,38], there are 7 target of interests in this

Table 2
RMSE values of all algorithms in AVIRIS data cube.

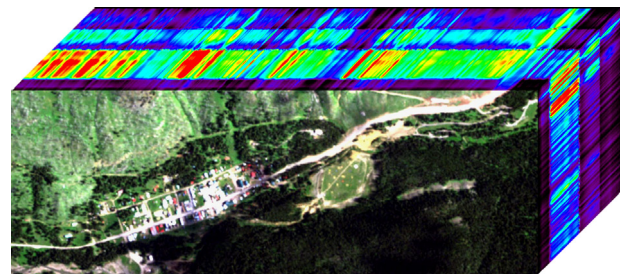|	PCA	MNF	TenD
RMSE	276.04	313.36	**194.45**

Fig. 3. HyMap data cube of the RIT project (bands 16, 8, and 1 for red, green, and blue, respectively). (For interpretation of the references to color in this figure caption, the reader is referred to the web version of this article.)

Table 1
SAM values between extracted endmembers in the original HSI and reconstructed data cubes.

ID	1#	2#	3#	4#	5#	6#	7#	8#	9#
PCA	**0.0113**	0.0162	0.0135	0.0261	0.0214	0.0122	0.0245	0.0158	0.0193
MNF	0.0174	0.0204	0.0142	0.0353	0.0245	0.0137	0.0286	0.0175	0.0209
TenD	0.0455	**0.0126**	**0.0075**	**0.0156**	**0.0171**	**0.0080**	**0.0146**	**0.0126**	**0.0165**

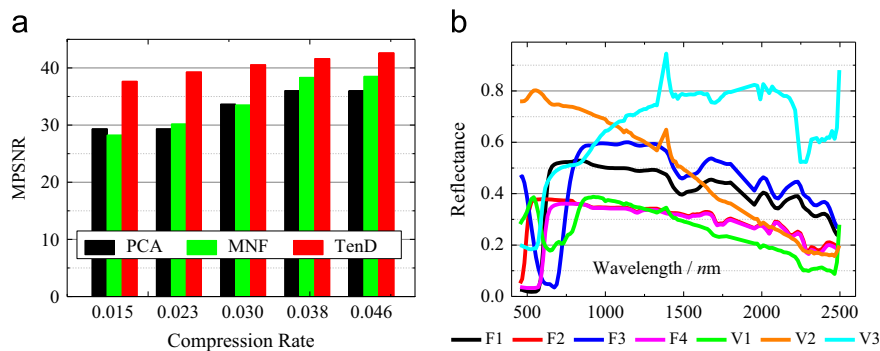| ID	10#	11#	12#	13#	14#	15#	16#	17#	18#
PCA	**0.0168**	0.0250	0.0148	0.0180	**0.0081**	0.0248	0.0223	0.0171	**0.0121**
MNF	0.0169	0.0267	0.0146	0.0184	0.0093	0.0272	0.0243	0.0164	0.0151
TenD	0.0285	**0.0166**	**0.0096**	**0.0095**	0.0088	**0.0129**	**0.0137**	**0.0161**	0.0136

Fig. 4. (a) MPSNR values with respect to various compression rates on HyMap data cube; (b) all target spectral curves equipped in SPL file.

Table 3
FARS values of all algorithms in HyMap data cube.

Target	F1	F2	F3	F4	V1	V2	V3
Original	2.90×10^{-4}	3.25×10^{-4}	1.15×10^{-2}	5.06×10^{-2}	2.83×10^{-2}	8.76×10^{-3}	5.93×10^{-2}
PCA	2.14×10^{-1}	2.26×10^{-1}	2.24×10^{-1}	2.91×10^{-1}	1.57×10^{-1}	1.05×10^{-1}	2.07×10^{-1}
MNF	2.31×10^{-1}	3.92×10^{-1}	2.63×10^{-1}	3.62×10^{-1}	1.21×10^{-1}	3.21×10^{-2}	1.74×10^{-1}
TenD	3.13×10^{-3}	9.67×10^{-3}	1.65×10^{-2}	7.82×10^{-2}	5.62×10^{-2}	2.46×10^{-2}	9.01×10^{-2}

HSI scene, including 4 fabrics and 3 vehicles, the prior spectra of which are obtained and preprocessed by the SPL files. In detail, the SPL spectra are rescaled according to its reflectance factor of 100 and resampled according to the HSI wavelength, the resulting spectra are shown in Fig. 4(b), and fed as the input of ACE. Since the true locations of all targets are known, the detection performance could be evaluated by the False Alarm Rate (FAR), which is defined as the number of non-target pixels that have an ACE output value equal to or higher than the true target pixel value, divided by the total number of pixels in the HSI. It is evident from Table 3 that the proposed algorithm gives a superior performance for all the targets in the HyMap experiment, but only a little higher than the original HSI by the FAR value.

4. Conclusion

This paper proposes an HSI compression and reconstruction algorithm by the tensor data processing approach. Since the HSI data is treated as a 3-order-tensor by which the spatial-spectral structure could be preserved as much as possible, we introduce a tensor decomposition technology to simultaneously project the original tensor into a core tensor with much lower dimensionality in each mode, by using the factor matrices, the HSI can be reconstructed by a simply multi-linear backward projection. Compared to the spectral DR based methods, the proposed TenD algorithm can significantly preserve the HSI data quality and present good performance in the following applications.

Acknowledgment

References

[1] A. Plaza, J.A. Benediktsson, J.W. Boardman, J. Brazile, L. Bruzzone, G. Camps-Valls, J. Chanussot, M. Fauvel, P. Gamba, A. Gualtieri, M. Marconcini, J.C. Tilton, G. Trianni, Recent advances in techniques for hyperspectral image processing, Remote Sens. Environ. 113 (1) (2009) 110–122.

[2] B. Zhang, X. Sun, L. Gao, L. Yang, Endmember extraction of hyperspectral remote sensing images based on the ant colony optimization (aco) algorithm, IEEE Trans. Geosci. Remote Sens. 49 (7) (2011) 2635–2646.

[3] B. Zhang, J. Gao, L. Gao, X. Sun, Improvements in the ant colony optimization algorithm for endmember extraction from hyperspectral images, IEEE J. Sel. Top. Appl. Earth Obs. Remote Sens. 6 (2) (2013) 522–530.

[4] J. Bioucas-Dias, A. Plaza, G. Camps-Valls, P. Scheunders, N. Nasrabadi, J. Chanussot, Hyperspectral remote sensing data analysis and future challenges, IEEE Geosci. Remote Sens. Mag. 1 (2) (2013) 6–36.

[5] X. Lu, H. Wu, Y. Yuan, P. Yan, X. Li, Manifold regularized sparse NMF for hyperspectral unmixing, IEEE Trans. Geosci. Remote Sens. 51 (5) (2013) 2815–2826.

[6] B. Du, L. Zhang, D. Tao, D. Zhang, Unsupervised transfer learning for target detection from hyperspectral images, Neurocomputing 120 (23) (2013) 72–82.

[7] B. Du, L. Zhang, Target detection based on a dynamic subspace, Pattern Recognit. 47 (1) (2014) 344–358.

[8] L. Zhang, L. Zhang, D. Tao, X. Huang, Sparse transfer manifold embedding for hyperspectral target detection, IEEE Trans. Geosci. Remote Sens. 52 (2) (2014) 1030–1043.

[9] W. Li, E.W. Tramel, S. Prasad, J.E. Fowler, Nearest regularized subspace for hyperspectral classification, IEEE Trans. Geosci. Remote Sens. 52 (1) (2014) 477–489.

[10] X. Kang, S. Li, J.A. Benediktsson, Spectral-spatial hyperspectral image classification with edge-preserving filtering, IEEE Trans. Geosci. Remote Sens. 52 (5) (2014) 2666–2677.

[11] L. Zhang, L. Zhang, D. Tao, X. Huang, On combining multiple features for hyperspectral remote sensing image classification, IEEE Trans. Geosci. Remote Sens. 50 (3) (2012) 879–893.

[12] Q. Du, J.E. Fowler, Hyperspectral image compression using jpeg 2000 and principal component analysis, IEEE Geosci. Remote Sens. Lett. 4 (2) (2007) 201–205.

[13] L. Zhang, X. Huang, Object-oriented subspace analysis for airborne hyperspectral remote sensing imagery, Neurocomputing 73 (4–6) (2010) 927–936.

[14] C.-I. Chang, Hyperspectral data exploitation: theory and applications, in: 3D Wavelet-based Compression of Hyperspectral Imagery, Wiley, NJ, 2007.

[15] B. Penna, T. Tillo, E. Magli, G. Olmo, Progressive 3-d coding of hyperspectral images based on jpeg 2000, IEEE Geosci. Remote Sens. Lett. 3 (1) (2006) 125–129.

[16] L. Wang, L. Jiao, J. Bai, J. Wu, Hyperspectral image compression based on 3d reversible integer lapped transform, Electron. Lett. 46 (24) (2010) 1601–1602.

[17] A. Karami, MehranYazdi, G. Mercier, Compression of hyperspectral images using discrete wavelet transform and tucker decomposition, IEEE J. Sel. Top. Appl. Earth Obs. Remote Sens. 5 (2) (2012) 444–450.

[18] Q. Du, W. Zhu, H. Yang, J.E. Fowler, Segmented principal component analysis for parallel compression of hyperspectral imagery, IEEE Geosci. Remote Sens. Lett. 6 (4) (2009) 713–717.

[19] W. Zhu, Q. Du, J.E. Fowler, Multitemporal hyperspectral image compression, IEEE Geosci. Remote Sens. Lett. 8 (3) (2011) 416–420.

[20] G. Motta, F. Rizzo, J.A. Storer, Hyperspectral image compression, in: An Architecture for the Compression of Hyperspectral Imagery, Springer-Verlag, NY, 2006.

[21] L.D. Lathauwer, Signal processing based on multilinear algebra (Ph.D. thesis), Katholike Universiteit Leuven, 1997.

[22] D. Muti, S. Bourennane, Multidimensional filtering based on a tensor approach, Signal Process. 85 (12) (2005) 2338–2353.

[23] D. Tao, X. Li, X. Wu, S. Maybank, Tensor rank one discriminant analysis—a convergent method for discriminative multilinear subspace selection, Neurocomputing 71 (10–12) (2008) 1866–1882.

[24] X. He, D. Cai, P. Niyogi, Tensor subspace analysis, in: Advances in Neural Information Processing Systems, vol. 17, MIT Press, Cambridge, MA, 2005, pp. 499–506.

[25] J. Dauwels, K. Srinivasan, M.R. Reddy, A. Cichocki, Near-lossless multichannel eeg compression based on matrix and tensor decompositions, IEEE J. Biomed. Health Inform. 17 (3) (2013) 708–714.

[26] Q. Zhang, H. Wang, R.J. Plemmonsz, V.P. Pauca, Tensor methods for hyperspectral data processing: a space object identification study, J. Opt. Soc. Am. A: Opt., Image Sci., Vis. 25 (12) (2008) 3001–3012.

[27] A. Karami, M. Yazdi, A.Z. Asli, Noise reduction of hyperspectral images using kernel non-negative tucker decomposition, IEEE J. Sel. Top. Signal Process. 5 (3) (2011) 487–493.

[28] D. Tao, X. Li, X. Wu, S.J. Maybank, General tensor discriminant analysis and Gabor features for gait recognition, IEEE Trans. Pattern Anal. Mach. Intell. 29 (10) (2007) 1700–1715.

[29] D. Tao, X. Li, X. Wu, W. Hu, S.J. Maybank, Supervised tensor learning, Knowl. Inf. Syst. 13 (1) (2007) 1–42.

[30] T.G. Kolda, B.W. Bader, Tensor decompositions and applications, SIAM Rev. 51 (3) (2009) 455–500.

[31] L.D. Lathauwer, B.D. Moor, J. Vandewalle, On the best rank-1 and rank-(r1, r2, …, rn) approximation of higher-order tensors, SIAM J. Matrix Anal. Appl. 21 (2001) 1324–1342.

[32] A.A. Green, M. Berman, P. Switzer, M.D. Craig, A transformation for ordering multispectral data in terms of image quality with implications for noise removal, IEEE Trans. Geosci. Remote Sens. 26 (1) (1988) 65–74.

[33] L. Gao, Q. Du, B. Zhang, W. Yang, Y. Wu, A comparative study on linear regression-based noise estimation for hyperspectral imagery, IEEE J. Sel. Top. Appl. Earth Obs. Remote Sens. 6 (2) (2013) 488–498.

[34] D. Snyder, J. Kerekes, I. Fairweather, R. Crabtree, J. Shive, S. Hager, Development of a web-based application to evaluate target finding algorithms, in: IEEE International Geoscience and Remote Sensing Symposium, 2008, pp. 915–918.

[35] J.M. Bioucas-Dias, J.M.P. Nascimento, Hyperspectral subspace identification, IEEE Trans. Geosci. Remote Sens. 46 (8) (2008) 2435–2445.

[36] J.M.P. Nascimento, J.M. Bioucas-Dias, Vertex component analysis: a fast algorithm to unmix hyperspectral data, IEEE Trans. Geosci. Remote Sens. 43 (4) (2005) 898–910.

[37] S. Kraut, L.L. Scharf, The CFAR adaptive subspace detector is a scale-invariant GLRT, IEEE Trans. Signal Process. 47 (9) (1999) 2538–2541.

[38] L. Zhang, L. Zhang, D. Tao, X. Huang, B. Du, Hyperspectral remote sensing image subpixel target detection based on supervised metric learning, IEEE Trans. Geosci. Remote Sens. 52 (8) (2014) 4955–4965.

Liangpei Zhang received the B.S. degree in physics from Hunan Normal University, Changsha, China, in 1982, the M.S. degree in optics from the Xian Institute of Optics and Precision Mechanics, Chinese Academy of Sciences, Xian, China, in 1988, and the Ph.D. degree in photogrammetry and remote sensing from Wuhan University, Wuhan, China, in 1998.
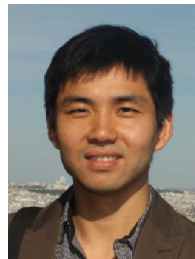
He is currently the Head of the Remote Sensing Division, State Key Laboratory of Information Engineering in Surveying, Mapping, and Remote Sensing, Wuhan University. He is also a Chang-Jiang Scholar Chair Professor appointed by the Ministry of Education of China. He is currently a Principal Scientist for the China State Key Basic Research Project (2011–2016) appointed by the Ministry of National Science and Technology of China to lead the remote sensing program in China. He has more than 300 research papers. He is the holder of five patents. His research interests include hyperspectral remote sensing, high-resolution remote sensing, image processing, and artificial intelligence.

Dacheng Tao received the B.Eng. degree from the University of Science and Technology of China, Hefei, China, the M.Phil. degree from The Chinese University of Hong Kong, Hong Kong, and the Ph.D. degree from the University of London, London, U.K.

He is a Professor of computer science with the Centre for Quantum Computation and Information Systems and the Faculty of Engineering and Information Technology, University of Technology, Sydney, Australia. He mainly applies statistics and mathematics for data analysis problems in data mining, computer vision, machine learning, multimedia, and video surveillance.

Xin Huang received the Ph.D. degree in Photogrammetry and Remote Sensing at the State Key Laboratory of Information Engineering in Surveying, Mapping and Remote Sensing (LIESMARS), Wuhan University, Wuhan, China, in 2009.

He is currently a full Professor at the LIESMARS, Wuhan University. His research interests include hyperspectral data analysis, high resolution image processing, pattern recognition and remote sensing applications. He has published more than 35 peer-reviewed papers in the international journals. He has frequently served as a referee for many international journals for remote sensing.

Bo Du received the B.S. degree from Wuhan Univeristy, Wuhan, China, in 2005, and received the Ph.D. degree in Photogrammetry and Remote Sensing from State Key Lab of Information Engineering in Surveying, Mapping and Remote Sensing, Wuhan University, Wuhan, China, in 2010.

He is currently an associate professor with the Computer School, Wuhan University, Wuhan, China. His major research interests include pattern recognition, hyperspectral image processing, and signal processing.

Lefei Zhang received the B.S. degree in sciences and techniques of remote sensing and the Ph.D. degree in photogrammetry and remote sensing from Wuhan University, Wuhan, China, in 2008 and 2013, respectively. In August 2013, He joined the Computer School, Wuhan University, where he is currently an Assistant Professor. His research interests include pattern recognition, machine learning, and remote sensing image processing.